Journal of Hydrology 614 (2022) 128584

Contents lists available at ScienceDirect

Journal of Hydrology

journal homepage: www.elsevier.com/locate/jhydrol

Research papers

Wavelet analysis of hydro-climatic time-series and vegetation trends of the Upper Aragón catchment (Central Spanish Pyrenees)

C. Juez [a,c,*], N. Garijo [b], E. Nadal-Romero [c], S.M. Vicente-Serrano [c]

[a] Estación Experimental de Aula Dei, Consejo Superior de Investigaciones Científicas (EEAD-CSIC), Zaragoza, Spain
[b] Universidad de Valladolid, Campus Universitario Duques de Soria, Soria, Spain
[c] Instituto Pirenaico de Ecología, Consejo Superior de Investigaciones Científicas (IPE-CSIC), Zaragoza, Spain

ARTICLE INFO

This manuscript was handled by Marco Borga, Editor-in-Chief, with the assistance of Marco Borga, Associate Editor.

Keywords:
River discharge
Climate change
Greenness
Wavelet analysis
Water management
Mediterranean catchments

ABSTRACT

Water managers and researchers noted with concern a nearly generalized decline in Mediterranean rivers discharge over the last decades. Changes in climatic forces (precipitation and air temperature) and land use and land cover (LULC) changes characterized by re-vegetation and greenness are the two most possible explanations for this discharge decline. The direct impact on river discharge stemming from these changes is difficult to assess and their role is generally studied separately. Here, we use the method of wavelet transformation to interpret the time-scale dependency of catchment discharge concerning the uneven temporal climatic fluctuations and re-vegetation processes. We analyzed the temporal variation of concurrent air temperature, precipitation and river discharge time-series for the Upper Aragón catchment, located in the Central Spanish Pyrenees. A long-term database collected over 60 years (1956–2020) was used. Land cover maps corresponding to different decades were used and the results indicated that the catchment experienced a significant increase in the area covered by mixed and broadleaf forests, mostly as a consequence of land abandonment. We show how temperature slightly increased and precipitation moderately decreased. However, catchment discharge experienced a sharp decline in its magnitude and also changes in its temporal variability dynamics. The relevance of the seasonal time-scales with regard to the available discharge is reduced, which strengthens the importance of the inter-annual time-scales for the catchment discharge dynamics. Furthermore, the catchment storage-discharge cycle at inter-annual time-scales is also reduced. Such changes can mostly be attributed to the changes in plant coverage, with an increasing weight in shaping hydrological processes at catchment scale due to the greenness effect. As such, we conclude that LULC changes have played a dominant role on the river discharge dynamics. Climatic trends, on the contrary, have been small, and they have played a secondary role in the decline of river discharge. Future research can use these observations to constrain the pace of upcoming water demands based on the available water resources at Mediterranean catchment scale.

1. Introduction

Discharge regime in most river catchments shows considerable variability at different time-scales: in the short-term (months, because of hydropower plants operations or snow melting due to the diurnal cycle), seasonally (summer and winter), annually (dry and wet periods) and in the long-term (multiannual trends). This fluctuation in discharge implies varying water resources, which may lead to problems in meeting water demand for agricultural purposes, hydropower or human consumption. This is an important challenge worldwide (Barnett et al., 2004; Black, 2016) and particularly in the Mediterranean area, where water is a scarce resource (García-Ruiz et al., 2011; López-Moreno et al., 2014). Mediterranean environments are primarily modulated by the water resources yielded by headwaters located in the upper mountainous regions. Such mountain areas are identified as wet islands or water towers within dry climate zones (Viviroli et al., 2007; Immerzeel et al., 2020) and they are highly vulnerable to climate change in a number of ways (Giorgi, 2006; European Environment Agency, 2015). Furthermore, most of the Mediterranean mountains have followed the historical land use and land cover (LULC) change: agricultural abandonment of the cultivated fields due to rural depopulation at the turn of the second half of the twentieth century and subsequent progressive (natural or man-

* Corresponding author at: Estación Experimental de Aula Dei, Consejo Superior de Investigaciones Científicas (EEAD-CSIC), Zaragoza, Spain.
E-mail address: carmelo.juez@ipe.csic.es (C. Juez).

https://doi.org/10.1016/j.jhydrol.2022.128584
Received 28 April 2022; Received in revised form 27 September 2022; Accepted 1 October 2022
Available online 29 October 2022

made) plant recolonization or afforestation (Lasanta et al., 2005; Lasanta et al., 2017; García-Ruiz and Lana-Renault, 2011). Therefore, the response of hydrological processes and water resources to global change need to be assessed in order to support and guide water policy and management practices in Mediterranean regions.

A great number of physical processes, acting at different and varying time-scales, influence in the discharge variability at the basin scale. Both climatic forces and vegetation are known as key drivers in river discharge dynamics (Beguería et al., 2003; Guardiola-Claramonte et al., 2011; Ficklin et al., 2018). Water resources for discharge and ultimately, for human purposes and freshwater ecosystems, depend on the partition of precipitation between runoff generation and water consumption by vegetation (Rulli et al., 2013). The changes in the relative importance of the partition of precipitation may thus provide information of the influence of climate change and land use and land cover change processes on the availability of water resources.

Climate projections indicate that periods with water deficits are expected to increase in frequency and severity in future decades in large regions of the world (Zhao and Dai, 2022; Hertig and Tramblay, 2017). Furthermore, radiative forcing increases atmospheric evaporative demand (Vicente-Serrano et al., 2020), which may also reinforce streamflow reduction in some regions (Vicente-Serrano et al., 2014). In parallel to this, there is an increase of water consumption by vegetation as consequence of greenness and re-vegetation processes (Mankin et al., 2018; Forzieri et al., 2020; Vicente-Serrano et al., 2021), which is also suggested to dominate available water for discharge in future climate change scenarios (Mankin et al., 2019). Nonetheless, other studies also advance that under elevated values of CO_2 plants display higher rates of photosynthesis, and decreased water use (Ainsworth & Rogers 2007). This in turn may have as a consequence an increase in soil moisture levels and runoff generation (Leakey et al., 2009). There is therefore a considerable debate and uncertainty about the role of climate and vegetation in the river catchment response to global change.

The analysis of hydro-climatic time-series to identify temporal patterns of discharge fluctuations, as well as their underlying drivers, is often based on standard statistical techniques, Fourier analysis or autoregressive models. The shortcoming of applying such analysis is that the identification of correlations of time-series require stationary relationships. However, on the basis of climate change and greenness process, we hypothesize that hydrological processes at river catchment scale change with time. Wavelet analysis takes into account non-stationary relationships among datasets (Torrence & Compo, 1998; Grinsted et al., 2004). Particularly, the continuous wavelet transform is a useful tool for the extraction of features, especially of complex time-series with a lot of noise. Furthermore, wavelet transform allows to time-localize the dominant time-scales within the complete temporal spectrum, ultimately identifying the variability of each time-scale all through the study period (contrary to Fourier spectral analysis or autoregressive analysis). Wavelet methodology was thus successfully used to analyze hydro-climatic time-series (Segele et al., 2009; Labat, 2010) or catchment temporal dynamics (Carey et al., 2013; Weigand et al., 2017; Pérez Ciria et al., 2019; Pérez Ciria and Chiogna, 2020; Juez & Nadal-Romero, 2021; Lorenzo-Lacruz et al., 2022).

In this study, the wavelet methodology in combination to traditional correlation analysis are applied to a long period database (1956–2000) with air temperature, precipitation and discharge records measured at six monitoring stations of the Upper Aragón catchment, located in the Central Spanish Pyrenees. This catchment underwent an intense process of re-vegetation for the last decades (Lasanta et al., 2005; García-Ruiz et al., 2015). We analyze the non-stationary impacts of climatic forces and re-vegetation processes on river discharge. We further hypothesized that, besides climatic trends (seasonal, annual), the major controlling factor of the variability and magnitude of discharge at river catchment are vegetation changes.

2. The Upper Aragón catchment and available data

2.1. The study area

The Upper Aragón catchment is located in the Central Spanish Pyrenees and it has an area of 2181 km^2 (see Fig. 1). The primary river of this catchment is the Aragón river, which starts at the Astún Valley, in the north of the catchment at an altitude of 2600 m a.s.l. The Aragón river flows north–south through the Canfranc valley and then turns to the west in Jaca. Downstream Jaca, the Aragón River heads west until reaching the end of the catchment, which coincides with the Yesa reservoir. The three main tributaries draining water to the catchment are: Subordán, Veral and Esca. Within the domain of the catchment (excluding the Yesa reservoir, located at the outlet) there are no dams or reservoirs and consequently, the river discharge follows a natural unmanaged regime.

The Upper Aragón catchment contains areas with limestone, sandstone, clay and marls. The catchment altitude ranges between 2600 m a.s.l. in the northernmost area and 500 m a.s.l. at Yesa Reservoir. The mean annual precipitation in the catchment is approximately 860 mm. Spring and autumn are the rainiest seasons. Summer is the driest season and it gets occasional storms due to convective processes. The average daily temperature in the catchment is 12 °C. Snow cover is found in high altitude, above the 1500 m a.s.l. from December to April (López-Moreno and García-Ruiz, 2004).

Vegetation cover in the catchment was strongly impacted by human activities. Historically, cultivated areas were located below 1600 m a.s.l., in the valley bottoms, flat areas and steep, south-facing hillslopes, which were managed even under shifting agriculture systems (Lasanta, 1998). Forests (*Pinus sylvestris*, *Fagus sylvatica*) are located on the north-facing slopes and everywhere between 1600 and 1800 m a.s.l. Between 1950 and 1960 most of the cultivated fields were abandoned, with the exception of those located in the valley bottom. The abandoned fields (which represent around 25 % of the catchment area) faced a process of greenness and plant re-colonization (Vicente-Serrano et al., 2006).

2.2. Air temperature, precipitation, discharge and land cover datasets

Daily discharge time-series data for the period 1956–2020 were obtained for six gauging stations: Aragón-Jaca, Subordán-Javierregay, Veral-Zuriza, Veral-Biniés, Esca-Sigüés and Aragón-Yesa (see Fig. 1 for the location and Table 1 for the main characteristics of each cathment). Discharge data were measured for the study period through the float method and water level probes. Rating curves were created based on the measurements. Data was available from the Ebro Water Authorities (CHE), https://www.chebro.es/.

Daily precipitation for the six gauging stations and air temperature for the Upper Aragón catchment were obtained from the Spanish National Meteorological Service (Agencia Estatal de Meteorología, AEMET). Further details about the processing methodology of this data set can be found in Vicente-Serrano et al. (2017). Given the time-scale analysis purposed in this study, we use the climatic time-series corresponding to the closest weather station to each gauging station.

Land use and land cover maps for the decades of 1960s and 2010s were provided by the Spanish Ministry of Agriculture. Based on interpreting aerial photographs and conducting fieldwork, these maps were created at a spatial scale of 1:50,000 (see Fig. 1). Furthermore, the Normalized Different Vegetation Index (NDVI) was used to infer consistent temporal vegetation growth and coverage dynamics. NDVI was calculated at a spatial resolution of 1.1 km using the NOAA-AVHRR images covering the period from 1982 to 2015 (Vicente-Serrano et al., 2020) combined with MODIS NDVI (Huete et al., 2002) for the period 2000–2020. Both datasets were standardized using the reference period 2000–2015 in order to provide homogeneous series that are not affected by the change of satellites.

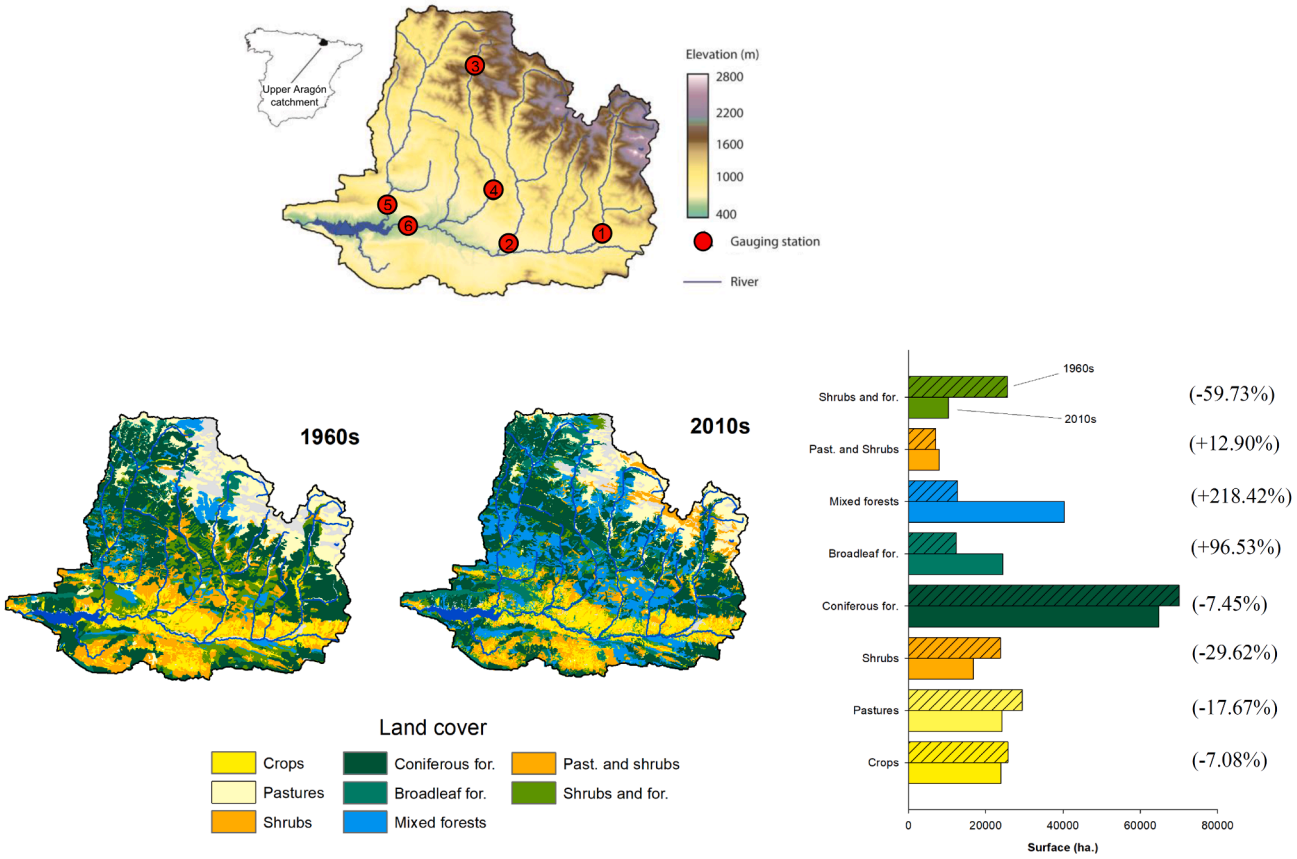

Fig. 1. The Upper Aragón catchment location and topography with the gauging stations (top). Land-cover categories for 1960 s and 2010 s. Percentage of changes is included between brackets (bottom).

Table 1
Main characteristics of the six gauging stations. Snow cover indicates whether the catchment area is occupied above 50% with snow during the winter period.

	ID Gaguing station	Altitude (m)	Minimum flow (m3/s)	Maximum flow (m3/s)	Mean flow (m3/s)	Snow cover
Aragón – Jaca	1	930	2.6	256.8	6.2	No
Subordán – Javierregay	2	810	3.5	300.1	11.0	No
Veral – Zuriza	3	1820	1.8	55.2	1.7	Yes
Veral – Biniés	4	780	1.9	102.2	4.1	No
Esca – Sigüés	5	630	2.2	256	10.3	No
Aragón – Yesa	6	560	1.9	797.26	31.7	No

3. Methods

3.1. Mann-Kendall test

The Mann-Kendall test is a classical statistical tool used in hydrological and climatic variables to assess whether a set of data values is increasing or decreasing over time, and whether the trend in either direction is statistically significant. Autocorrelation was considered in the trend analysis. This test was used with a twofold purpose: (i) to detect significant long-term trends in the database; and (ii) to assess the impact of greenness and re-vegetation processes on long-term trends for two equally spaced periods (1956–1988 and 1989–2020). These two periods correspond to different vegetation levels. The first period, 1956–1988, corresponds to the early land abandonment process and further process of secondary succession of shrubs followed by trees. A natural vegetation cover colonized most of the former cultivated fields (which represent around 25 % of the catchment area, see Vicente-Serrano et al., (2006)). Furthermore, slopes and terraces were afforested for economic and environmental purposes. The second period, 1989–2020, corresponds to a period with small changes in relation to the area of abandoned fields. This period is characterized by a consolidation process of the greenness expansion triggered during previous years, with well-rooted and mature vegetation. The surface occupied by mixed and broadleaf forests is significantly increased for the 1989–2020 period (see Fig. 1).

3.2. Wavelet analysis

Air temperature, precipitation and discharge time-series are rarely stationary and they consist of a broad set of transient patterns varying within the temporal record. The wavelet transform allows to localize in both time and periodicity the transient patterns recorded in such non-stationary time-series. It thus provides a complete time-scale representation of localized and transient phenomena occurring at different time-scales (Torrence & Compo, 1998). In this research, we make use of the Morlet wavelet, which was successfully used in the past to analyze precipitation and discharge time-series (Carey et al., 2013; Labat et al., 2005; Juez and Nadal-Romero, 2021; Juez et al., 2021). This wavelet type is characterized as:

$$\varphi_0(\eta) = \pi^{-1/4} e^{i\omega_0\eta} e^{-\eta^2/2} \quad (1)$$

where $\varphi_0(\eta)$ is the wavelet function,η, is a dimensionless time parameter, i is the imaginary unit and ω_0 is the dimensionless angular frequency taken as 6 which provides a right match between time and frequency localization. Thus, for a time-series X_n for each scale s at all n of series length N, the wavelet function is mathematically represented as:

$$W_n(s) = \sum_{n'=0}^{N-1} x_{n'} \psi^* \left[\frac{(\eta' - \eta)\Delta t}{s} \right] \quad (2)$$

where $W_n(s)$ is the wavelet transform coefficients, ψ the normalized wavelet, (*) the complex conjugate, s the wavelet scale, n the localized time index and n' the translated time index of the time ordinate x. It is possible to reconstruct the original signal by summing each time-scale.

In addition, to study the interaction between two time-series, we also compute a bivariate framework called squared wavelet coherence (Grinsted et al., 2004), which compares two wavelet spectra corresponding to two time-series. The square wavelet coherence measures the local linear correlation between two time-series, X and Y, with wavelet transforms $W_n^X(s)$ and $W_n^Y(s)$ at each time-scale. Hence, it is analogous to the squared correlation coefficient in linear regression. Because of these characteristics, the squared wavelet coherence can identify regions in the time–space where the examined time-series co-move, but do not necessarily have a high common power. We compute the squared wavelet coherence coefficients following the approach of Grinsted et al. (2004):

$$R_n^2(S) = \frac{|S(s^{-1} W_n^{XY}(S))|^2}{S\left(s^{-1}|W_n^X(s)|^2\right) \cdot S\left(s^{-1}|W_n^Y(s)|^2\right)} \quad (3)$$

being S a smoothing operator for both scale and time domain.

$$S(W) = S_{scale}(S_{time}(W_n(s))) \quad (4)$$

where S_{time} smooths along the time axis and S_{scale} smooths along the scale axis. The squared wavelet coherence coefficient is in the range $0 \leq R_n^2(s) \leq 1$. Values close to zero indicate weak correlation, while values close to one provide evidence of strong correlation. Hence, we discarded values where $R_n^2(s) < 0.5$ to avoid non-reliable estimations.

Finally, to complete the analysis, the wavelet coherence phase difference is also computed to provide details on the oscillation (cycles) between two time-series (see Lee and Kim, 2019). The phase difference is calculated as follows:

$$\phi_n [\text{unknown template}] \quad (5)$$

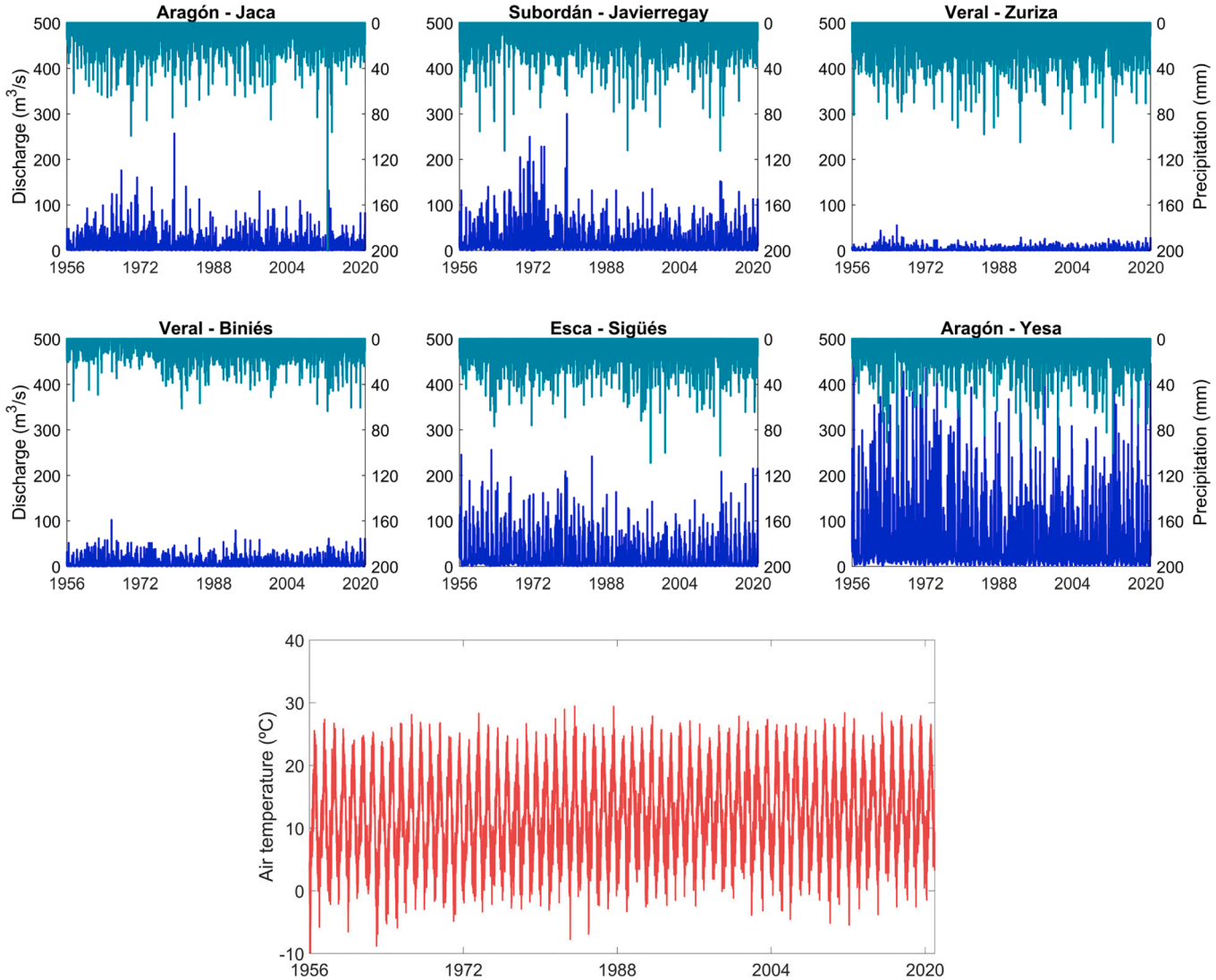

Fig. 2. Time-series of daily precipitation and discharge records (top) and of daily temperature records (bottom) for the period 1956–2020 and for the study sites.

where *Im(S(W)* and *Re(S(W))* represent the imaginary and real part of *S (W)*, respectively. The phase differences are explained as the differences of both correlation and lagging relationships. For example, if the difference is zero, the two time-series are perfectly correlated and they move together. Values of phase difference in the interval [−*90*; *90*] indicate the two time-times are correlated. Values of phase difference between the interval [−90;−180] or between [90;180] indicate the two time-series are anti-correlated. Considering the correlation of our time-series (i.e. phase difference within the interval [−*90*; *90*]), the phase difference can be explained as the phase lagging (negative values, the first time-series lags the second one) or phase leading (positive values, the first time-series leads the second one) at specific time-scales.

4. Results

4.1. Temporal spectrum analysis

Precipitation patterns depict similar dynamics for the six catchment locations (see Fig. 2-top). Rainiest seasons are spring (March-June) and autumn (October-December). Discharge response patterns show similarities in temporal variability (low flow during winter and summer and peak flow during late spring) and differences in magnitude between gauging locations. Discharge records are lower at Veral-Zuriza and Veral-Biniés, as these gauging stations are located at the headwaters and the drainage area is smaller. Conversely, discharge records at Aragón-Yesa are maximal because this downstream location drains water from the entire catchment. Fig. 2-bottom displays the time-series of air temperature for the river catchment. An episodic pattern of increasing and

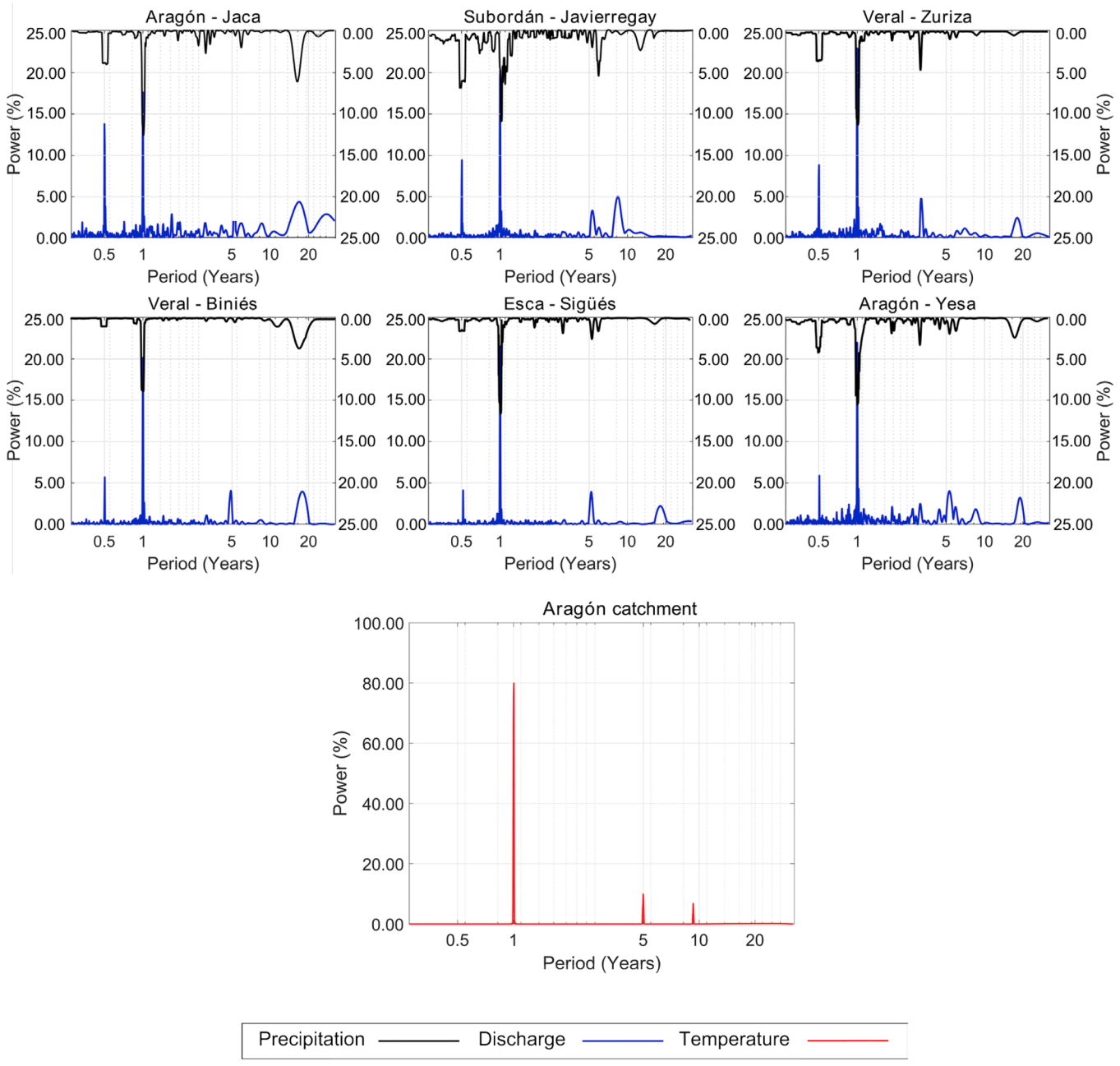

Fig. 3. Spectral characteristics of precipitation and discharge (top) and air temperature (bottom) time-series for the Upper Aragón catchment recorded for the period 1956–2020. The global wavelet periodogram (local wavelet power averaged over 1956–2020) is expressed as percentage of total global power summed over all periods.

decreasing temperature all through each year of the study period is observed.

Fig. 3 shows the corresponding global wavelet periodogram for precipitation, discharge and air temperature time-series (local wavelet power is displayed in Fig. S1 of the supporting material). This analysis allows to identify the non-overlapping dominant time-scales governing the temporal records, based on the peaks with larger amplitude. Precipitation and discharge response features intra-seasonal (0.003–0.5 years), annual (1-year period), short-term-annual (1.1–5.5 years) and long-term-annual (5.5–20 years) episodic patterns. Moreover, the air temperature response features three dominant time-scales related with annual (1 year period), short-term-annual (1.1–5.5 years) and long-term-annual (5.5–20 years) episodic patterns. In all the time-series, the annual cycle contains the dominant power. Furthermore, there is also a strong variability around a time-scale of 0.5 years for the precipitation and discharge time-series. This effect is further accentuated in the discharge response patterns, where the time-scale of 0.5 years peaks with higher power than in the precipitation response patterns. The hydrological cycle of the Aragón catchment is thus identified as a bi-modal cycle with high flow seasons observed each year for two periods: spring

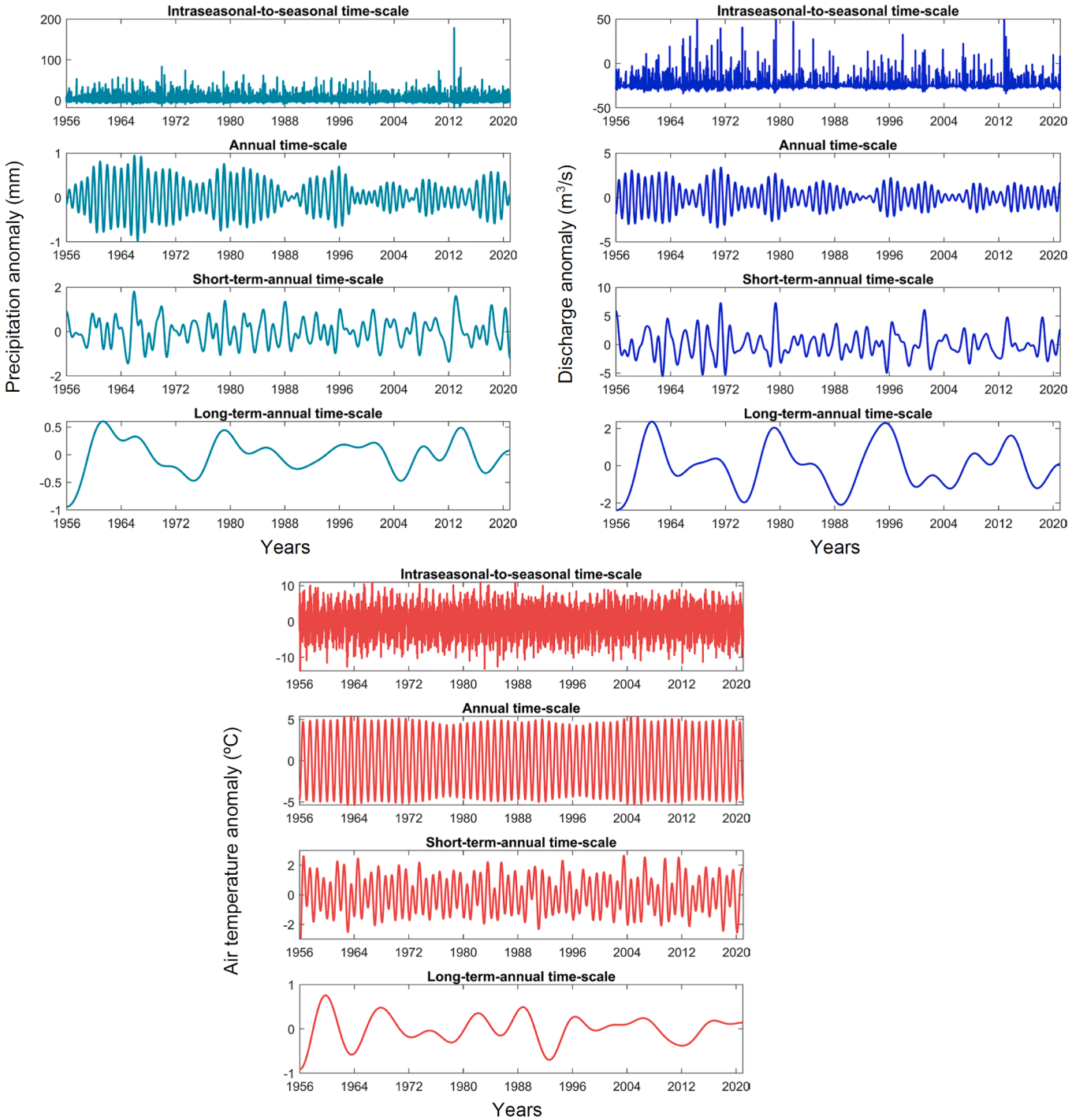

Fig. 4. Temporal scale-by-scale de-composition of daily precipitation, discharge and air temperature time-series anomalies for the Aragón-Jaca gauging station. Positive and negative anomalies are calculated with respect to the mean values. The four non-overlapping time-scales bands contain the major power peaks and were determined based on the global power spectra displayed in Fig. 3. Note: scales are different for each variable.

(March-June) and autumn (October-December).

Fig. 4 displays the temporal scale-by-scale de-composition of daily precipitation, discharge and air temperature time-series anomalies for the Aragón-Jaca gauging station. Temporal anomalies for the other gauging stations are similar and are displayed in Fig. S2 of the supporting information for the sake of brevity. The non-overlapping time-scale bands in Fig. 4 contain the major power peaks and are identified based on the global power spectra plotted in Fig. 3. Positive and negative anomalies are calculated with respect to the mean values. Precipitation time-series exhibit similar trends for the intraseasonal-to-seasonal, short-term and long-term annual time-scales. Differences are found in the annual time-scales where it can be seen a slight decrease for the 1989–2020 period with respect to 1956–1988 period. Regarding the discharge time-series, for the annual and short-term time-scales a reduction in the magnitude of the anomalies are observed for the 1989–2020 period. Furthermore, for the 1989–2020 period the short-term annual time-scale anomalies vary more slowly (in a longer period of years), and thus attenuate the contribution of the short-term-annual time-scale in the discharge. Finally, air temperature anomalies depict similar trends for all the time-scales.

Temporal dynamics of the Upper Aragón catchment are further analyzed by means of the percentage of changes computed for the 1956–2020 period (see Table 2). The increase in air temperature is observed all through the study period and it is statistically significant. Precipitation shows a slight decrease in all the gauging stations, except in Subordán-Javierregay, where a subtle increase is observed. These changes are not statistically significant in the majority of the gauging stations. Discharge shows a strong and statistically significant reduction in all the measuring stations except in Veral-Zuriza, where an important increase is recorded. The strong discharge reduction (ranging between −19 to −48 %) is not explained by the precipitation reduction (ranging between −8 to −13 %). Furthermore, discharge reduction is more severe

Table 2
Summary of the temporal evolution of the annual precipitation, discharge and air temperature values for three time periods: 1956–2020, 1956–1988 and 1989–2020. Percentage of changes was calculated from the linear regression lines obtained by means of least-squares. Negative percentages are colored in red and positive percentages are colored in green. P-values were calculated by means of the Mann-Kendall test. P-values in bold within a shaded cell indicate significance for a 95% confidence level.

	Time period					
	1956-2020		1956-1988		1989-2020	
	Q (m^3/s)	P (mm)	Q (m^3/s)	P (mm)	Q (m^3/s)	P (mm)
Aragón - Jaca						
Mean	6.20	2.30	7.12	2.45	5.27	2.14
Change (%)	-25.98	-12.57	-16.00	-6.06	-11.89	-6.93
p-value	**0.01**	0.26	**0.01**	0.42	0.09	0.13
Subordán - Javierregay						
Mean	11.01	2.25	12.84	2.18	9.18	2.32
Change (%)	-28.50	6.19	-21.95	0.99	-8.39	5.15
p-value	**0.01**	**0.03**	**0.03**	0.54	0.19	0.09
Veral - Zuriza						
Mean	1.89	3.33	1.74	3.47	2.04	3.19
Change (%)	17.24	-8.04	20.40	-6.78	6.19	-1.35
p-value	**0.01**	0.54	0.11	0.66	0.54	0.06
Veral - Biniés						
Mean	4.12	2.05	4.54	2.22	3.69	1.87
Change (%)	-18.72	-15.51	-12.25	-5.62	-7.31	-10.52
p-value	**0.02**	0.32	0.13	**0.04**	0.27	0.51
Esca - Sigüés						
Mean	10.39	2.32	12.53	2.43	8.24	2.20
Change (%)	-34.24	-9.49	-23.20	-2.33	-14.37	-7.33
p-value	**0.01**	0.58	**0.01**	0.96	0.17	0.37
Aragón Yesa						
Mean	24.55	2.25	32.28	2.40	16.82	2.09
Change (%)	-47.89	-13.07	-38.10	-9.85	-15.82	-3.57
p-value	**0.01**	0.49	**0.01**	0.83	0.16	0.96
	Temp. (°C)		**Temp. (°C)**		**Temp. (°C)**	
Upper Aragón Catchment						
Mean	12.13		11.40		12.86	
Change (%)	11.31		10.83		11.81	
p-value	**0.03**		**0.02**		**0.03**	

for the period 1956–1988 and for all the gauging stations. Specifically, the highest discharge reduction is observed at Aragón-Yesa. This gauging station is located at the outlet of the river catchment and consequently, amplifies any discharge change observed in the drainage area.

Table 2 also shows the mean values for the 1956–1988 and 1989–2020 periods. Discharge shows a larger decline for the first time period (decline ranging between −12 to −38 %), with regard to the second period (decline ranging between −7 to −16 %) and with the exception of Veral-Zuriza (increase of 20 and 6 % for the first and second period, respectively).

Table 3 displays the standard deviation change for precipitation, discharge and air temperature time-series for the 1956–1988 and 1989–2020 periods. We used the standard deviation as a proxy to measure the magnitude of the anomalies in relation to the mean of the whole 1956–2020 period. Subsequently, we computed the standard deviation change to assess any variability (in other words, any irregularity/deviation) between the two study periods. An increase in the magnitude of the standard deviation (i.e. more extreme values) of precipitation is observed at the intraseasonal time-scale for all the gauging stations. Furthermore, looking at the mean values of the Aragón catchment, we observe higher standard deviation values for all the time-scales for the 1989–2020 period. This implies that anomalies in relation to the mean are more spread out and extreme events occurred more often. Discharge values show a decrease in the standard deviation values for the 1989–2020 period and for all the time-scales. The largest drop in the standard deviation values is noted for the intraseasonal and annual time-scales. Lastly, air temperature values show a slight increase in the standard deviation values for the intraseasonal values (i.e. larger differences in temperature between winter and summer) and a notable drop in the long-term time-scale (i.e. a steady climatic trend is observed).

Fig. 5 displays the temporal evolution of the NDVI values computed for the Upper Aragón catchment and for the 1982–2020 period. Complete annual information before 1982 is not available, as the first NOAA-AVHRR satellite was launched in July 1981. NDVI shows a linear increase. In parallel, the standard deviation for each year was also computed and overlapped in the figure. The standard deviation depicts a decline from 1986 to 1988 to 2020.

Table 3
Summary of the standard deviation change for precipitation, discharge and air temperature time-series and for the 1956–1988 and 1989–2020 periods. Percentage of changes were obtained by applying the standard statistical deviation formula to each wavelet time-scale (intraseasonal, annual, short-term and long-term) and to each study period. Mean values for the Upper Aragón catchment were also computed and included.

Time-scale	Standard deviation change between 1956 and 1988 & 1989–2020 periods (%)			
	Intraseasonal	Annual	Short-term	Long-term
Precipitation				
Aragón – Jaca	5.25	−28.04	−8.96	0.41
Subordán – Javierregay	18.12	24.32	14.83	10.53
Veral – Zuriza	2.40	−18.18	−6.33	−35.79
Veral – Biniés	28.22	−18.75	−0.83	−33.01
Esca – Sigüés	15.77	19.81	26.49	35.98
Aragón Yesa	22.51	22.04	25.90	33.66
Mean Upper Aragón Catchment	15.38	1.87	8.52	8.63
Discharge				
Aragón – Jaca	−23.76	−42.42	−16.45	−12.50
Subordán – Javierregay	−31.01	−24.48	−11.68	−13.64
Veral – Zuriza	−15.64	−15.66	−13.67	−11.02
Veral – Biniés	−12.88	−5.03	− 4.35	−18.02
Esca – Sigüés	−27.19	−21.51	−15.47	−12.99
Aragón Yesa	−18.88	−18.83	−10.91	−11.44
Mean Upper Aragón Catchment	−21.56	−19.64	−12.10	−13.33
Air temperature				
Mean Upper Aragón Catchment	−3.73	−0.91	−0.04	−21.31

4.2. Significant wavelet coherence between hydro-climatic time-series

The squared wavelet coherence between air temperature and discharge (see Fig. 6-a) displays strong wavelet coherence for seasonal and annual time-scales before and after 1988 (local squared wavelet coherence values are displayed in Fig. S3). This is not surprising given the high synchronicity in the annual dynamics of air temperature and resulting discharge. High air temperatures during summer foster evaporation and water consumption by plants. As a result, available discharge is reduced in the whole catchment. On the other hand, the second period of study displays significant wavelet coherence for the long-term time-scale (around 10-years). This indicates that the dependency between years with abnormally high/low air temperatures and discharge is accentuated for the 1989–2020 period. Conversely, the squared wavelet coherence between precipitation and discharge (see Fig. 6-b) also shows strong wavelet coherence for seasonal and annual time-scales before and after 1988. However, a significant shift in the wavelet coherence is observed in the 3–12 years range: for 1956–1988 the maximum peaks are clustered around time-scales of 5–12 years range and for 1989–2020 the maximum peaks are clustered around time-scales of 3–5 years range.

Phase differences for the six gauging stations and for the two study periods are displayed in Figs. 7 and 8. Air temperature and discharge time-series (see Fig. 7) are anti-correlated for annual time-scales (phase difference interval between [−180; −90]), which implies that as air temperature increases the discharge magnitude is reduced. Furthermore, the 1989–2020 period shows two distinct trends with regard to the 1956–2020 period. First, looking at intraseasonal time-scales, at Veral-Zuriza gauging station the discharge time-series peaks before the air temperature time-series. Second, a delay between both time-series is observed at short-term time-scales (around 5-years). The continuous and regular increase of air temperature for the study period (around 1.2 °C) fosters the melting of traditionally perennial snow package located in the northernmost sector of the catchment and provides additional interannual discharge variability.

Precipitation and discharge time-series (see Fig. 8) show a delay in discharge response with regard to precipitation for all the time-scales. Conversely, three notable differences are found between the two study periods. One is that at intraseasonal time-scales, the delay between precipitation and discharge is larger for the 1989–2020 period. The second point is that at annual time-scales the delay between precipitation and discharge time-series is slightly decreased in the 1989–2020 period in relation to the 1956–1988 period. The last point is that while a certain level of variability is observed at time-scales larger than 1-year for the 1956–1988 period, those time-scales show similar trends for the 1989–2020 period.

5. Discussion

The analysis of long-term data of precipitation, air temperature and discharge time-series is used to interpret the impacts of climate variability and generalized re-vegetation and greenness observed at the Upper Aragón catchment in relation to discharge dynamics. Examination of the temporal structure of the datasets reveals dominant time-scales accounting for seasonal, annual, short-term-annual and long-term annual time-scales.

The seasonal (peaks around 0.5 years) and annual time-scales reflect a bi-modal cycle with high flow seasons observed each year for two periods: spring (March-June) and autumn (October-December). These characteristics of the yearly discharge distribution reflect that the Upper

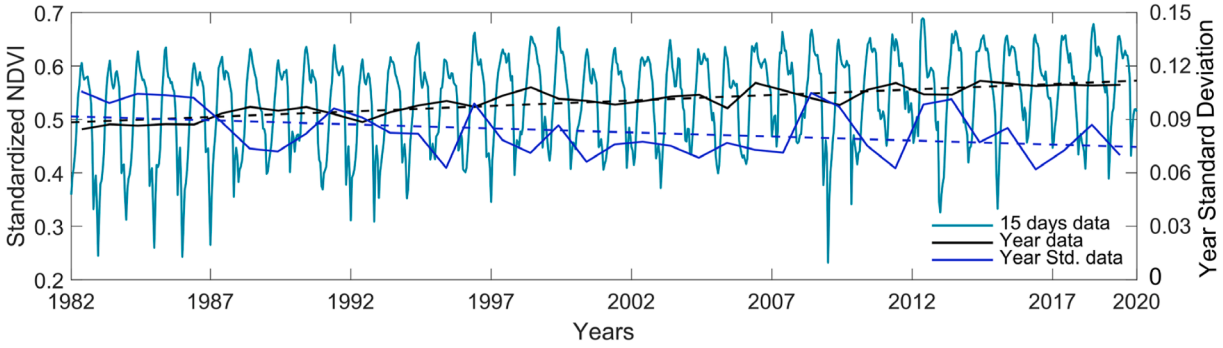

Fig. 5. Temporal evolution of the NDVI over the Upper Aragón Catchment for the 1982–2020 period. Standard deviation for the intra-annual NDVI values are also included. Dashed lines are the regression fits obtained by means of least-squares.

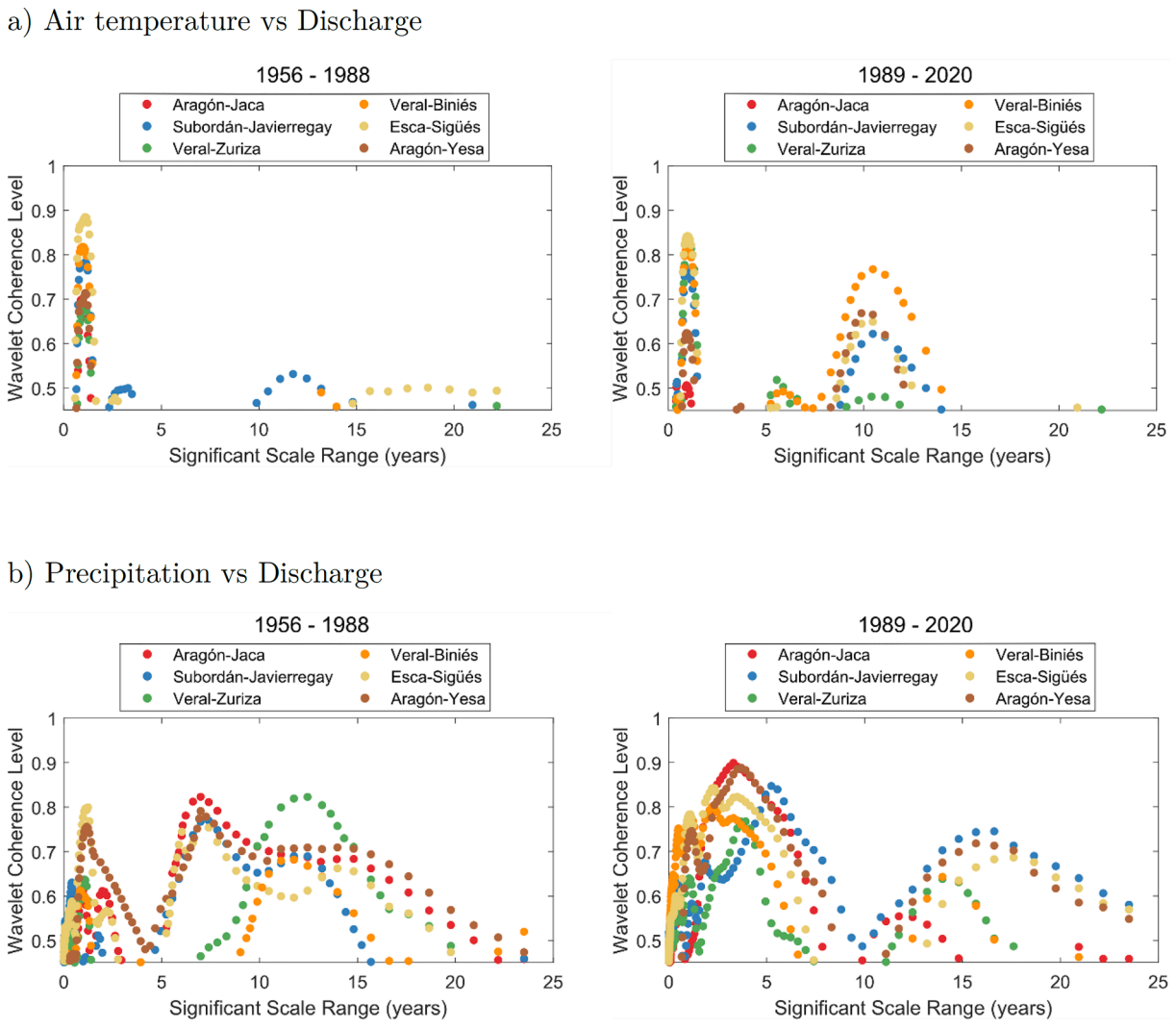

Fig. 6. Significant squared wavelet coherence levels between air temperature and discharge (top) and between precipitation and discharge (bottom) for the two study periods: 1956–1988 and 1989–2020.

Aragón catchment follows mainly a precipitation hydrological regime (with dry and wet periods) but it is also partially modulated by the snow-melting cycle of the headwaters in spring. Snow usually accumulates between December and April and it melts down during May (López-Moreno et al., 2013; López-Moreno et al., 2020). The melting process of the winter snowpack notably contributes to the high-flow season observed during late spring or early summer. Conversely, the interannual time-scales (greater than1 year) are mainly related to long-term anomalies in the precipitation and flow events. The role of these interannual time-scales is of particular interest because their contribution fluctuates between transient periods of positive and negative values.

On the other hand, magnitude and variability of the time-series do not remain stationary and differences were found. Initially we computed

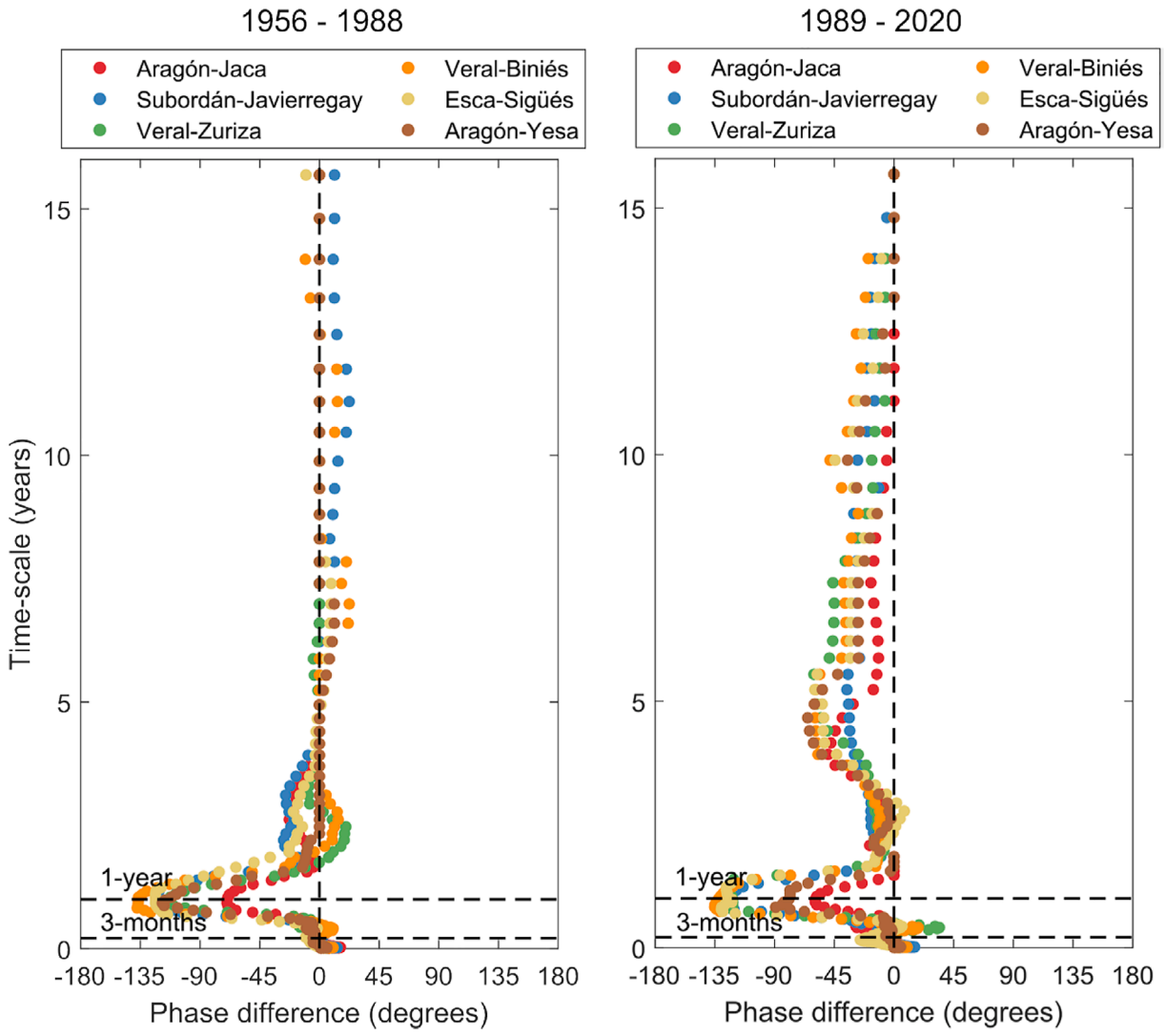

Fig. 7. Phase difference angle distributions between the air temperature and discharge time-series for the two study periods and for the six gauging stations.

the observed changes for the 1956–2020 period and we found that: (i) air temperature was statistically significant increased in the catchment by 1.2 °C; (ii) precipitation rates were moderately and non-statistically significant reduced (ranging between −8 to −16 %). These precipitation trends are in agreement with observations over the western Mediterranean region, which are characterized by dominant internal variability of precipitation and non-significant long-term trends (Peña-Angulo et al., 2020); and (iii) discharge values were strongly and statistically significant reduced (ranging between −19 to −48 %) with the exception of Veral-Zuriza. This increase in discharge at Veral-Zuriza (the gauging station is located at a high elevation, 1800 m ab.s.l., in the northernmost part of the catchment and hence snow covers a larger percentage of the drained area, see Fig. 1) is related with the increase of air temperature which favors the melting of snow package at the Pyrenees and provides extra water resources to the river catchment (Vidaller et al., 2021). The strong decline in discharge observed in the rest of the gauging stations cannot be attributed to drops in precipitation, which are in a moderate reduction. Furthermore, these discharge trends are in agreement with the trend observed in other natural non-managed catchments in Spain (Lorenzo-Lacruz et al., 2012; Martínez-Fernández et al., 2013; Vicente-Serrano et al., 2020). In these studies, authors attributed the decrease in water yield to the generalized greenness process, as a result of land abandonment. Results herein outlined confirm that the increase of dense vegetation (mixed and broadleaf forests) corresponds with a decrease in discharge magnitude and also, that precipitation trends play a secondary role in this discharge alteration (non-significant non-statistically significant correlation and moderate alterations). Furthermore, vegetation age may also affect the identified processes. Discharge reduction is more pronounced for the 1956–1988 period (characterized by shrubs and young trees) with regard to the 1989–2020 period (characterized by mixed and broadleaf trees). This is in agreement with previous studies, which conclude that young forests consume more water than old-growth forests (Delzon and Loustau, 2005; Ellison et al., 2017; Teuling and Hoek van Dijke, 2020).

The importance of re-vegetation and greenness on the available water resources in the Aragón catchment is further stressed with the standard deviation change, which is computed for the temporal anomalies before and after 1988 (see Table 3). Increase of precipitation standard deviation is observed on average for the Upper Aragón catchment for all the time-scales, being the seasonal time-scale the one with a larger increase (around + 15 %). In contrast, larger reductions in the discharge standard deviation (around −20 %) are observed for seasonal and annual time-scales. These reductions in the magnitude of discharge anomalies are related with the increasing modulating impact of the biophysical mechanisms of plants (due to the increment of greenness, see NDVI values in Fig. 5): during summer season, water consumption by plants is increased and during winter season, photosynthesis and transpiration processes by plants are reduced and so is the water

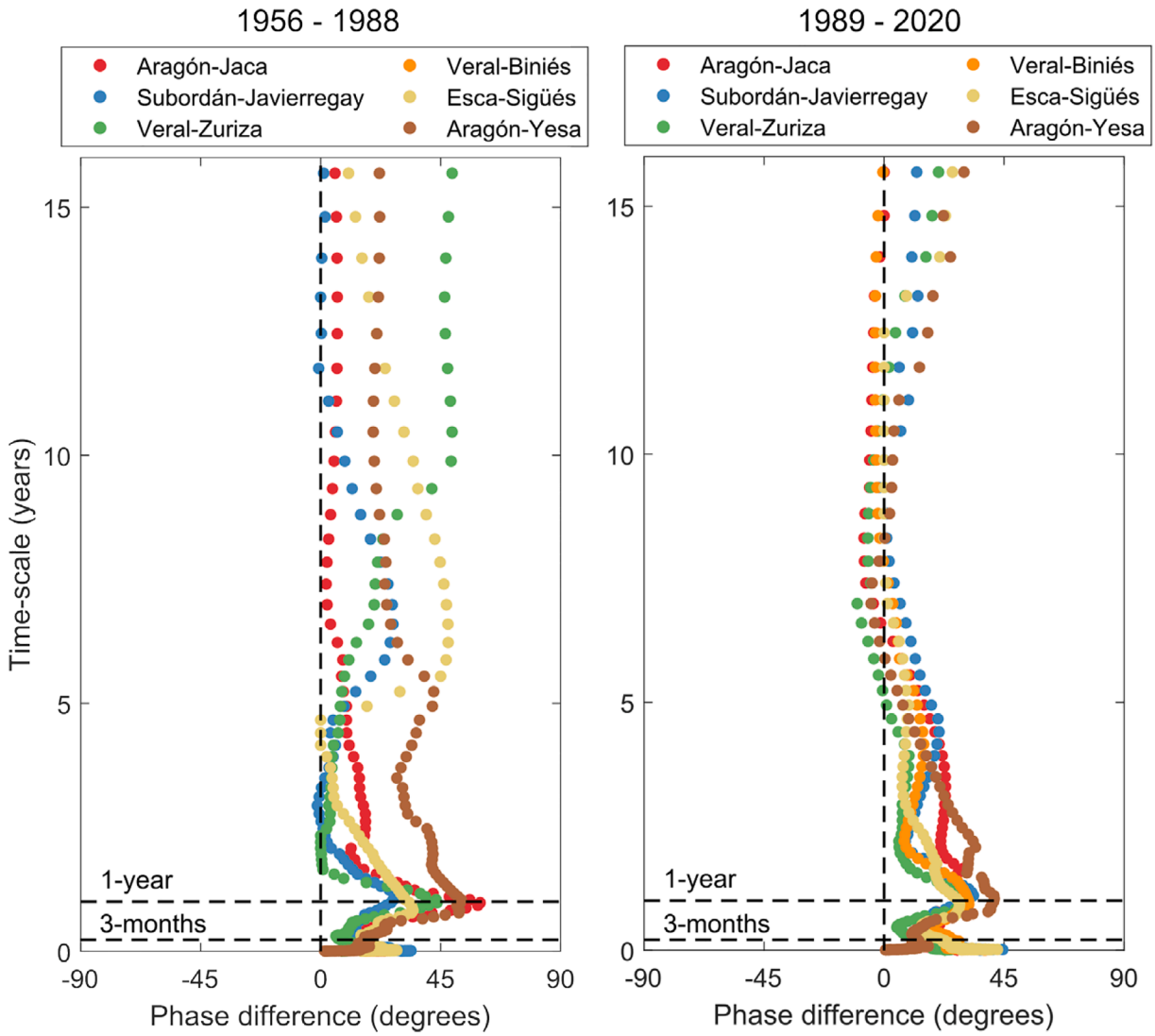

Fig. 8. Phase difference angle distributions between the precipitation and discharge time-series for the two study periods and for the six gauging stations.

consumption. The increase of NDVI values runs in parallel to the intra-annual NDVI standard deviation decline (see Fig. 5). We thus show how the vegetation dynamics dominate the catchment discharge response at seasonal and annual time-scales, compared to the precipitation dynamics.

An additional interesting point about the differences in discharge dynamics before and after 1988 is the temporal shift in the wavelet coherence between precipitation and discharge time-series at interannual time-scales, from the 5–12 years range (1956–1988 period) to the 3–7 years range (1989–2020), as well as stronger coherence values for the 1989–2020 period (see Fig. 6-b). This different trend is explained based on two points. One is that seasonal precipitation standard deviation change shows an increase for 1989–2020 (around 15 %, see Table 3). This precipitation standard deviation increase at seasonal time-scales is linked to more severe and intermittent droughts (Vicente-Serrano et al., 2014). The relevance of the seasonal timescales with regard to the available discharge is thus reduced, which strengthens the importance of the inter-annual time-scales for the catchment discharge dynamics. These inter-annual time-scales have the mission to recharge the water reserves of the catchment, by which the discharge will be fed in the following years (Wang, 2012; Velasco et al., 2017; Juez and Nadal-Romero, 2020). The second point is that the greenness process observed all across the catchment has decreased the measured (and visible) discharge but it may have favored the groundwater discharge. Tree root architecture enhances hydraulic redistribution of water in soils (Prieto et al., 2012). Thereby, old-growth trees (which correspond to the 1989–2020 period) maximize groundwater recharge (Ilstedt et al., 2016). Wavelet coherence at inter-annual time-scales supports this point. The catchment storage-discharge cycle at inter-annual time-scales was reduced from the 5–12 years range (1956–1988 period) to the 3–7 years range (1989–2020). In other words, the temporal shift in the strong linear correlation between precipitation and discharge at inter-annual time-scales is due to the fact that water catchment reserves are filled in a shorter period of time.

Phase difference response between precipitation and discharge time-series (see Fig. 8) is also a good proxy to understand the importance of vegetation on the catchment discharge. At intraseasonal time-scales, the delay between precipitation and discharge is larger for the 1989–2020 period. This is explained by the fact that the general re-vegetation and greenness processes observed in the entire catchment modulate the response to precipitation (van Noordwijk et al., 2016). Plants, especially tree roots, enhance soil permeability (Keeler et al., 2019). Consequently, infiltration processes are increased and resulting runoff is reduced. This point helps to recharge groundwater and to mitigate floods (Grey et al., 2018). Furthermore, at annual time-scales the delay between precipitation and discharge time-series is slightly decreased in the 1989–2020 period in relation to the 1956–1988 period. This may indicate that re-vegetation and greenness processes have favored the hydrological

connectivity within the catchment (trees improve soil structure and permeability, channeling underground water (Miyata et al. 2019), and ultimately, have reduced the asynchrony between precipitation and discharge peaks.

The abandonment of cultivated areas in the Upper Aragón catchment resulted in the loss of the traditional rural mosaic (with a more variable vegetation structure) and lead to a process of greenness and plant re-colonization which implies a more homogeneous landscape (Lasanta et al., 2017; Mantero et al., 2020). Looking at the phase difference response between precipitation and discharge time-series in Fig. 8, we observe a remarkable homogenization trend for the 1989–2020 period with regard to the previous period and for all the study sites and time-scales. We thus believe that this markedly changes in the coupling between precipitation and discharge was owned by a process of vegetation homogenization in the whole catchment.

Results herein described are in line with previous research on river headwaters in Spain, where a statistically significant discharge decline was observed during the last decades (Lorenzo-Lacruz et al., 2012; Martínez-Fernández et al., 2013). Therefore, these results emphasize the need of implementing management policies for water-limited environments, such as the mountain areas in Mediterranean regions. Traditional river catchment management is based on the capacity of water managers to meet water demand based on historical discharge patterns (Capon et al., 2018). However, projected climate and LULC scenarios in Mediterranean catchments (see García-Ruiz et al., 2011) suggest: (i) a continuous air temperature increase (1–6 °C); (ii) a decline in precipitations for the 21st century; and (iii) an intense greenness processes, with a significant upward shift of the upper treeline in most headwaters areas (Manrique-Alba et al., 2022). This last point reveals critical in light of our results. For this reason, although water managers have no control on the climatic forces, they can promote land management practices to reduce water consumption by vegetation. In this regard, silviculture practices such as clearing shrublands for livestock (Lasanta et al., 2017), thinning to adapt dense stands of trees to available water resources (Manrique-Alba et al., 2020) or uneven-aged silviculture systems (Aszalós et al., 2022) may be considered as needed tools for catchment management in mountain Mediterranean areas.

6. Conclusions

The temporal structure of concurrent air temperature, precipitation and discharge time-series at the Upper Aragón catchment was herein analyzed by means of the wavelet analysis. The long-term dataset combined with land cover maps and NDVI time-series allow to explore the nature of discharge patterns and relate them to catchment and river processes occurring at different and non-similar time-scales.

In this catchment, discharge experiences a dramatic drop in its magnitude for the study period and also changes in its temporal variability dynamics. Variability in climatic forces and LULC changes due to re-vegetation and greenness are targeted as two possible explanations for this discharge decline. The results illustrate that discharge reduction is mainly caused by the biophysical processes of plants, with an increasing weight in shaping hydrological processes at catchment scale due to the greenness effect. Climatic fluctuations, on the contrary, play a secondary role and are only responsible of the partial decline in river discharge magnitude.

CRediT authorship contribution statement

C. Juez: Conceptualization, Methodology, Writing – original draft. **N. Garijo:** Conceptualization, Methodology, Writing – review & editing. **E. Nadal-Romero:** Conceptualization, Writing – review & editing. **S.M. Vicente-Serrano:** Conceptualization, Writing – review & editing.

Declaration of Competing Interest

The authors declare that they have no known competing financial interests or personal relationships that could have appeared to influence the work reported in this paper.

Data availability

Data will be made available on request.

Acknowledgments

This work was funded by the H2020-MSCA-IF-2018 programme (Marie Sklodowska-Curie Actions) of the European Union under REA grant agreement, number 834329-SEDILAND. Data presented in this manuscript will be uploaded at an open repository if the paper is accepted for publication.

Appendix A. Supplementary data

Supplementary data to this article can be found online at https://doi.org/10.1016/j.jhydrol.2022.128584.

References

Ainsworth, E.A., Rogers, A., 2007. The response of photosynthesis and stomatal conductance to rising (CO2): mechanisms and environmental interactions. Plant, Cell Environ. 30, 258–270.

Aszalós, R., Thom, D., Aakala, T., Angelstam, P., Brümelis, G., Gálhidy, L., Gratzer, G., Hlásny, T., Katzensteiner, K., Kovács, B., Knoke, T., Larrieu, L., Motta, R., Müller, J., Ódor, P., Rożenbergar, D., Paillet, Y., Pitar, D., Standovár, T., Svoboda, M., Szwagrzyk, J., Toscani, P., Keeton, W.S., 2022. Natural disturbance regimes as a guide for sustainable forest management in Europe. Ecol. Appl. 32 (5).

Barnett, T., Malone, R., Pennell, W., Stammer, D., Semtner, B., Washington, W., 2004. The effects of climate change on water resources in the west: introduction and overview. Clim. Change 62 (1), 1–11.

Beguería, S., López-Moreno, J.I., Lorente, A., Seeger, M., García-Ruiz, J.M., 2003. Assessing the effect of climate oscillations and land-use changes on streamflow in the Central Spanish Pyrenees. Ambio 32 (4), 283–286. https://doi.org/10.1579/0044-7447-32.4.283.

Black, M., 2016. The atlas of water: mapping the World's most critical resource. Univ of California Press.

Capon, S.J., Leigh, C., Hadwen, W.L., George, A., McMahon, J.M., Linke, S., Reis, V., Gould, L., Arthington, A.H., 2018. Transforming environmental water management to adapt to a changing climate. Front. Environ. Sci. 6 https://doi.org/10.3389/fenvs.2018.00080.

Carey, S.K., Tetzlaff, D., Buttle, J., Laudon, H., McDonnell, J., McGuire, K., Seibert, J., Soulsby, C., Shanley, J., 2013. Use of color maps and wavelet coherence to discern seasonal and interannual climate influences on streamflow variability in northern catchments. Water Resour. Res. 49 (10), 6194–6207.

Delzon, S., Loustau, D., 2005. Age-related decline in stand water use: sap flow and transpiration in a pine forest chronosequence. Agric. For. Meteorol. 129 (3–4), 105–119. https://doi.org/10.1016/j.agrformet.2005.01.002.

Ellison, D., Morris, C.E., Locatelli, B., Sheil, D., Cohen, J., Murdiyarso, D., Gutierrez, V., Noordwijk, M.V., Creed, I.F., Pokorny, J., Gaveau, D., Spracklen, D.V., Tobella, A.B., Ilstedt, U., Teuling, A.J., Gebrehiwot, S.G., Sands, D.C., Muys, B., Verbist, B., Springgay, E., Sugandi, Y., Sullivan, C.A., 2017. Trees, forests and water: Cool insights for a hot world. Global Environ. Change 43, 51–61.

European Environment Agency, 2015. Mediterranean Sea region briefing – The European environment — state and outlook 2015. Source: European Environment Agency www.eea.europa.eu/soer/2015/countries/mediterranean.

Ficklin, D.L., Abatzoglou, J.T., Robeson, S.M., Null, S.E., Knouft, J.H., 2018. Natural and managed watersheds show similar responses to recent climate change. PNAS 115 (34), 8553–8557.

Forzieri, G., Miralles, D.G., Ciais, P., Alkama, R., Ryu, Y., Duveiller, G., Zhang, K.e., Robertson, E., Kautz, M., Martens, B., Jiang, C., Arneth, A., Georgievski, G., Li, W., Ceccherini, G., Anthoni, P., Lawrence, P., Wiltshire, A., Pongratz, J., Piao, S., Sitch, S., Goll, D.S., Arora, V.K., Lienert, S., Lombardozzi, D., Kato, E., Nabel, J.E.M. S., Tian, H., Friedlingstein, P., Cescatti, A., 2020. Increased control of vegetation on global terrestrial energy fluxes. Nat. Clim. Change 10 (4), 356–362.

García-Ruiz, J.M., Lana-Renault, N., 2011. Hydrological and erosive consequences of farmland abandonment in Europe, with special reference to the Mediterranean region - A review. Agric. Ecosyst. Environ. 140 (3–4), 317–338.

García-Ruiz, J.M., López-Moreno, J.I., Vicente-Serrano, S.M., Lasanta–Martínez, T., Beguería, S., 2011. Mediterranean water resources in a global change scenario. Earth Sci. Rev. 105 (3-4), 121–139.

García-Ruiz, J.M., López-Moreno, J.I., Lasanta, T., Vicente-Serrano, S.M., González-Sampériz, P., Valero-Garcés, B.L., Sanjuán, Y., Beguería, S., Nadal-Romero, E., Lana-

Renault, N., Gómez-Villar, A., 2015. Geo-ecological effects of global change in the Central Spanish Pyrenees: A review at different spatial and temporal scales. Pirineos 170. https://doi.org/10.3989/Pirineos.2015.170005.
Giorgi, F., 2006. Climate change hot-spots. Geophys. Res. Lett. 33 (8).
Grey, V., Livesley, S.J., Fletcher, T.D., Szota, C., 2018. Tree pits to help mitigate runoff in dense urban areas. J. Hydrol. 565, 400–410. https://doi.org/10.1016/j.jhydrol.2018.08.038.
Grinsted, A., Moore, J.C., Jevrejeva, S., 2004. Application of the cross wavelet transform and wavelet coherence to geophysical time series. Nonlinear Processes of Geophysics 11, 561–566. https://doi.org/10.5194/npg-11-561-2004.
Guardiola-Claramonte, M., Troch, P.A., Breshears, D.D., Huxman, T.E., Switanek, M.B., Durcik, M., Cobb, N.S., 2011. Decreased streamflow in semi-arid basins following drought-induced tree die-off: A counter-intuitive and indirect climate impact on hydrology. J. Hydrol. 406 (3), 225–233. https://doi.org/10.1016/j.jhydrol.2011.06.017.
Hertig, E., Tramblay, Y., 2017. Regional downscaling of Mediterranean droughts under past and future climatic conditions. Global Planet. Change 151, 36–48.
Huete, A., Didan, K., Miura, T., Rodriguez, E.P., Gao, X., Ferreira, L.G., 2002. Overview of the radiometric and biophysical performance of the MODIS vegetation indices. Remote Sens. Environ. 83 (1–2), 195–213. https://doi.org/10.1016/S0034-4257(02)00096-2.
Ilstedt, U., Bargués Tobella, A., Bazié, H.R., Bayala, J., Verbeeten, E., Nyberg, G., Sanou, J., Benegas, L., Murdiyarso, D., Laudon, H., Sheil, D., Malmer, A., 2016. Intermediate tree cover can maximize groundwater recharge in the seasonally dry tropics. Sci. Rep. 6 (1).
Immerzeel, W.W., Lutz, A.F., Andrade, M., Bahl, A., Biemans, H., Bolch, T., Hyde, S., Brumby, S., Davies, B.J., Elmore, A.C., Emmer, A., Feng, M., Fernández, A., Haritashya, U., Kargel, J.S., Koppes, M., Kraaijenbrink, P.D.A., Kulkarni, A.V., Mayewski, P.A., Nepal, S., Pacheco, P., Painter, T.H., Pellicciotti, F., Rajaram, H., Rupper, S., Sinisalo, A., Shrestha, A.B., Viviroli, D., Wada, Y., Xiao, C., Yao, T., Baillie, J.E.M., 2020. Importance and vulnerability of the world's water towers. Nature 577 (7790), 364–369.
Juez, C., Nadal-Romero, E., 2020. Long-term time-scale bonds between discharge regime and catchment specific landscape traits in the Spanish Pyrenees. Environ. Res. 191, 110158 https://doi.org/10.1016/j.envres.2020.110158.
Juez, C., Nadal-Romero, E., 2021. Long-term temporal structure of catchment sediment response to precipitation in a humid mountain badland area. J. Hydrol. 597, 125723 https://doi.org/10.1016/j.jhydrol.2020.125723.
Juez, C., Garijo, N., Hassan, M.A., Nadal-Romero, E., 2021. Intraseasonal-to-Interannual Analysis of Discharge and Suspended Sediment Concentration Time-Series of the Upper Changjiang (Yangtze River). Water Resour. Res. 57 (8), e2020WR029457.
Keeler, B.L., Hamel, P., McPhearson, T., Hamann, M.H., Donahue, M.L., Meza Prado, K.A., Arkema, K.K., Bratman, G.N., Brauman, K.A., Finlay, J.C., Guerry, A.D., Hobbie, S.E., Johnson, J.A., MacDonald, G.K., McDonald, R.I., Neverisky, N., Wood, S.A., 2019. Social-ecological and technological factors moderate the value of urban nature. Nat. Sustainability 2 (1), 29–38.
Labat, D., 2010. Cross wavelet analyses of annual continental freshwater discharge and selected climate indices. J. Hydrol. 385 (1–4), 269–278.
Labat, D., Ronchail, J., Guyot, J.L., 2005. Recent advances in wavelet analyses: Part 2: Amazon, Parana, Orinoco and Congo discharges time scale variability. J. Hydrol. 314 (1-4), 289–311.
Lasanta, T., 1998. The process of desertion of cultivated areas in the Central Spanish Pyrenees. Pirineos 132, 15–36.
Lasanta, T., Vicente-Serrano, S., Cuadrat, J., 2005. Mountain Mediterranean landscape evolution caused by the abandonment of traditional primary activities: a study of the Spanish Central Pyrenees. Appl. Geogr. 25, 47–65. https://doi.org/10.1016/j.apgeog.2004.11.001.
Lasanta, T., Arnáez, J., Pascual, N., Ruiz-Flaño, P., Errea, M.P., Lana-Renault, N., 2017. Space–time process and drivers of land abandonment in Europe. Catena 149, 810–823. https://doi.org/10.1016/j.catena.2016.02.024.
Leakey, A.D., Ainsworth, E.A., Bernacchi, C.J., Rogers, A., Long, S.P., Ort, D.R., 2009. Elevated CO2 effects on plant carbon, nitrogen, and water relations: six important lessons from FACE. J. Exp. Bot. 60 (10), 2859–2876.
Lee, E., Kim, S., 2019. Wavelet analysis of soil moisture measurements for hillslope hydrological processes. J. Hydrol. 575, 82–93. https://doi.org/10.1016/j.jhydrol.2019.05.023.
López-Moreno, J.I., García-Ruiz, J.M., 2004. Influence of snow accumulation and snowmelt on streamflow in the central Spanish Pyrenees. Hydrol. Sci. J. 49 (5) https://doi.org/10.1623/hysj.49.5.787.55135.
López-Moreno, J.I., Soubeyroux, J.M., Gascoin, S., Alonso-Gonzalez, E., Durán-Gómez, N., Lafaysse, M., Vernay, M., Carmagnola, C., Morin, S., 2020. Long-term trends (1958–2017) in snow cover duration and depth in the Pyrenees. Int. J. Climatol. 40 (14), 6122–6136.
López-Moreno, J.I., Vicente-Serrano, S.M., Zabalza, J., Beguería, S., Lorenzo-Lacruz, J., Azorin-Molina, C., Morán-Tejeda, E., 2013. Hydrological response to climate variability at different time scales: A study in the Ebro basin. J. Hydrol. 477, 175–188. https://doi.org/10.1016/j.jhydrol.2012.11.028.
López-Moreno, J.I., Zabalza, J., Vicente-Serrano, S.M., Revuelto, J., Gilaberte, M., Azorin-Molina, C., Morán-Tejeda, E., García-Ruiz, J.M., Tague, C., 2014. Impact of climate and land use change on water availability and reservoir management: Scenarios in the Upper Aragón River, Spanish Pyrenees. Sci. Total Environ. 493, 1222–1231.
Lorenzo-Lacruz, J., Vicente-Serrano, S.M., López-Moreno, J.I., Morán-Tejeda, E., Zabalza, J., 2012. Recent trends in Iberian streamflows (1945–2005). J. Hydrol. 414, 463–475. https://doi.org/10.1016/j.jhydrol.2011.11.023.
Lorenzo-Lacruz, J., Morán-Tejeda, E., Vicente-Serrano, S.M., Hannaford, J., García, C., Peña-Angulo, D., Murphy, C., 2022. Streamflow frequency changes across western Europe and interactions with North Atlantic atmospheric circulation patterns. Global Planet. Change 212.
Mankin, J.S., Seager, R., Smerdon, J.E., Cook, B.I., Williams, A.P., Horton, R.M., 2018. Blue water trade-offs with vegetation in a CO2-enriched climate. Geophys. Res. Lett. 45 (7), 3115–3125. https://doi.org/10.1002/2018GL077051.
Mankin, J.S., Seager, R., Smerdon, J.E., Cook, B.I., Williams, A.P., 2019. Mid-latitude freshwater availability reduced by projected vegetation responses to climate change. Nat. Geosci. 12 (12), 983–988.
Manrique-Alba, À., Beguería, S., Molina, A.J., González-Sanchis, M., Tomàs-Burguera, M., del Campo, A.D., Colangelo, M., Camarero, J.J., 2020. Long-term thinning effects on tree growth, drought response and water use efficiency at two Aleppo pine plantations in Spain. Sci. Total Environ. 728 https://doi.org/10.1016/j.scitotenv.2020.138536.
Manrique-Alba, À., Beguería, S., Camarero, J.J., 2022. Long-term effects of forest management on post-drought growth resilience: An analytical framework. Sci. Total Environ. 810, 152374 https://doi.org/10.1016/j.scitotenv.2021.152374.
Mantero, G., Morresi, D., Marzano, R., Motta, R., Mladenoff, D.J., Garbarino, M., 2020. The influence of land abandonment on forest disturbance regimes: a global review. Landscape Ecol. 35 (12), 2723–2744.
Martínez-Fernández, J., Sánchez, N., Herrero-Jiménez, C.M., 2013. Recent trends in rivers with near-natural flow regime: The case of the river headwaters in Spain. Prog. Phys. Geogr. 37 (5), 685–700.
Miyata, S., Gomi, T., Sidle, R.C., Hiraoka, M., Onda, Y., Yamamoto, K., Nonoda, T., 2019. Assessing spatially distributed infiltration capacity to evaluate storm runoff in forested catchments: Implications for hydrological connectivity. Sci. Total Environ. 669, 148–159.
Peña-Angulo, D., Vicente-Serrano, S.M., Domínguez-Castro, F., Murphy, C., Reig, F., Tramblay, Y., Trigo, R.M., Luna, M.Y., Turco, M., Noguera, I., Aznárez-Balta, M., García-Herrera, R., Tomas-Burguera, M., El Kenawy, A., 2020. Long-term precipitation in Southwestern Europe reveals no clear trend attributable to anthropogenic forcing. Environ. Res. Lett. 15 (9), 094070.
Pérez Ciria, T., Chiogna, G., 2020. Intra-catchment comparison and classification of long-term streamflow variability in the Alps using wavelet analysis. J. Hydrol. 587.
Pérez Ciria, T., Labat, D., Chiogna, G., 2019. Detection and interpretation of recent and historical streamflow alterations caused by river damming and hydropower production in the Adige and Inn river basins using continuous, discrete and multiresolution wavelet analysis. J. Hydrol. 578.
Prieto, I., Armas, C., Pugnaire, F.I., 2012. Water release through plant roots: new insights into its consequences at the plant and ecosystem level. New Phytol. 193 (4), 830–841.
Rulli, M.C., Saviori, A., D'Odorico, P., 2013. Global land and water grabbing. Proc. Natl. Acad. Sci. 110 (3), 892–897.
Segele, Z., Lamb, P., Leslie, L., 2009. Seasonal-to-interannual variability of Ethiopia/Horn of Africa monsoon. Part I: Associations of wavelet-filtered large-scale atmospheric circulation and global sea surface temperature. J. Clim. 22, 3396–3421. https://doi.org/10.1175/2008JCLI2859.1.
Teuling, A.J., Hoek van Dijke, A.J., 2020. Forest age and water yield. Nature 578 (7794), E16–E18. https://doi.org/10.1038/s41586-020-1941-5.
Torrence, C., Compo, G.P., 1998. A Practical Guide to Wavelet Analysis. Bull. Am. Meteorol. Soc. 79, 61–78. https://doi.org/10.1175/1520-0477(1998)079.
van Noordwijk, M., Tanika, L., Lusiana, B., 2016. Flood risk reduction and flow buffering as ecosystem services: a flow persistence indicator for watershed health. Hydrol. Earth Syst. Sci. Discuss. https://doi.org/10.5194/hess-2015-538.
Velasco, E.M., Gurdak, J.J., Dickinson, J.E., Ferré, T.P.A., Corona, C.R., 2017. Interannual to multidecadal climate forcings on groundwater resources of the US West Coast. J. Hydrol.: Reg. Stud. 11, 250–265. https://doi.org/10.1016/j.ejrh.2015.11.018.
Vicente-Serrano, S.M., Beguería, S., Lasanta, T., 2006. Diversidad espacial de la actividad vegetal en el Pirineo Central Español: análisis de los procesos de sucesión mediante imágenes Landsat (1984–2001). Pirineos 161, 59–84.
Vicente-Serrano, S.M., Azorin-Molina, C., Sanchez-Lorenzo, A., Revuelto, J., López-Moreno, J.I., González-Hidalgo, J.C., Moran-Tejeda, E., Espejo, F., 2014a. Reference evapotranspiration variability and trends in Spain, 1961–2011. Global Planet. Change 121, 26–40.
Vicente-Serrano, S.M., Domínguez-Castro, F., Murphy, C., Peña-Angulo, D., Tomas-Burguera, M., Noguera, I., López-Moreno, J.I., Juez, C., Grainger, S., Eklundh, L., Conradt, T., Azorin-Molina, C., Kenawy, A., 2021. Increased vegetation in mountainous headwaters amplifies water stress during dry periods. Geophys. Res. Lett. 48 (18) https://doi.org/10.1029/2021GL094672.
Vicente-Serrano, S.M., Lopez-Moreno, J.-I., Beguería, S., Lorenzo-Lacruz, J., Sanchez-Lorenzo, A., García-Ruiz, J.M., Azorin-Molina, C., Morán-Tejeda, E., Revuelto, J., Trigo, R., Coelho, F., Espejo, F., 2014b. Evidence of increasing drought severity caused by temperature rise in southern Europe. Environ. Res. Lett. 9 (4), 044001 https://doi.org/10.1088/1748-9326/9/4/044001.
Vicente-Serrano, S.M., Tomas-Burguera, M., Beguería, S., Reig, F., Latorre, B., Peña-Gallardo, M., Luna, M.Y., Morata, A., González-Hidalgo, J.C., 2017. A high resolution dataset of drought indices for Spain. Data 2 (3), 22.
Vicente-Serrano, S.M., McVicar, T.R., Miralles, D.G., Yang, Y., Tomas-Burguera, M., 2020. Unraveling the influence of atmospheric evaporative demand on drought and its response to climate change. WIREs Clim. Change 11, e632.
Vidaller, I., Revuelto, J., Izagirre, E., Rojas-Heredia, F., Alonso-González, E., Gascoin, S., René, P., Berthier, E., Rico, I., Moreno, A., Serrano, E., Serreta, A., López-Moreno, J.I., 2021. Toward an ice-free mountain range: demise of Pyrenean glaciers during 2011–2020. Geophys. Res. Lett. 48 (18).

Viviroli, D., Dürr, H.H., Messerli, B., Meybeck, M., Weingartner, R., 2007. Mountains of the world, water towers for humanity: Typology, mapping, and global significance. Water Resour. Res. 43 (7) https://doi.org/10.1029/2006WR005653.

Wang, D., 2012. Evaluating interannual water storage changes at watersheds in Illinois based on long-term soil moisture and groundwater level data. Water Resour. Res. 48 (3) https://doi.org/10.1029/2011WR010759.

S. Weigand R. Bol B. Reichert A. Graf I. Wiekenkamp M. Stockinger A. Luecke W. Tappe H. Bogena T. Puetz W. Amelung H. Vereecken Spatiotemporal analysis of dissolved organic carbon and nitrate in waters of a forested catchment using wavelet analysis Vadose zone journal 16 3 2017 10.2136/vzj2016.09.0077 vzj2016.09.0077.

Zhao, T., Dai, A. (2022). CMIP6 Model-Projected Hydroclimatic and Drought Changes and Their Causes in the Twenty-First Century. *Journal of Climate. American Meteorological Society*, Boston MA, USA 35(3): 897–921. DOI: 10.1175/JCLI-D-21-0442.1.